Preprint Title Liver-Targeting Nanoparticles of iron oxide (Fe_3O_4) and their complexes with phytopreparation for the biocompatibility

Authors Shushanik A. Kazaryan, Seda A. Oganian, Gayane S. Vardanyan, Anatolie S. Sidorenko and Ashkhen A. Hovhannisyan

Publication Date 29 Juli 2024

Article Type Full Research Paper

ORCID® iDs Anatolie S. Sidorenko - https://orcid.org/0000-0001-7433-4140; Ashkhen A. Hovhannisyan - https://orcid.org/0000-0001-6828-0588

Liver-Targeting Nanoparticles of iron oxide (Fe_3O_4) and their complexes with phytopreparation for the biocompatibility

Kazaryan Sh.A.[1], Oganian S.A. [1], Vardanyan G.S.[2], Sidorenko A.S.[3], Hovhannisyan A.A.*[1]

[1]Department of Medical Biochemistry and Biotechnology, Russia-Armenian (Slavonic) University, Armenia, Yerevan, H.Emin str., 123

[2]Yerevan State Medical University After M. Heraci, Department of Biochemistry, Koryun 2, Yerevan, Yerevan, Armenia

[3]Ghitu Institute of Electronic Engineering and Nanotechnologies of Technical University of Moldova, Chisinau, Moldova

Email: Hovhannisyan Ashkhen - ashkhen.hovhannisyan@rau.am

* Corresponding author

Abstract

Thanks to their simple synthesis, controlled physical properties, and minimal toxicity, iron oxide nanoparticles (Fe_3O_4 NPs) are widely used in many biomedical applications (bioimaging, drug delivery, biosensors, diagnostics, theranostics, etc.). However, the use of NPs does not preclude the possibility of some selective toxicity and undesirable effects, including their accumulation in tissues and direct interaction with specific biological targets. This study evaluated the biocompatibility of Fe_3O_4 NPs, *Teucrium polium* (*T. polium)* extract, rutin, and their complexes on the liver tissue of healthy white Wistar rats.

The impact profile of the synthesized Fe_3O_4 NPs (15 ± 4 nm), rutin, *T. polium* extract, and their complexes on biochemical markers of liver function (ALT, AST, ALP, GGT, HDL, LDL, total cholesterol, total protein, albumin) and morphological indicators of rat liver was investigated. Fe_3O_4 NPs, rutin, and *T. polium* extract do not have direct hepatotoxicity when administered i/p to rats, unlike their complexes. All agents exert a hypolipidemic effect by lowering LDL, despite maintaining the synthetic functions of the liver. Fe_3O_4 NPs increase the activity of GPO, which is associated with their peroxidase-like properties. A multifaceted and diverse mechanism of action of all studied samples on the liver of Wistar rats was identified.

Keywords

iron oxide (Fe_3O_4) nanoparticle; *T. polium*; rutin; hepatotoxicity; biocompatibility

Introduction

Leveraging nanotechnology, personalized medicine, and interdisciplinary collaboration is essential for overcoming the complex challenges associated with human health. The development of nanotechnology has provided resources for various applications in the medical field, leading to significant advances in diagnosis, biological detection, therapy, and drug delivery [1].

Iron oxide nanoparticles, due to their minimal toxicity, are considered the most preferred agents for studying various biomedical applications [2]. There are many studies proving the biocompatibility of iron NPs, and due to their unique magnetic, paramagnetic, and other properties, Fe_3O_4 NPs have great potential for commercial use and have already found applications in biomedicine as contrast enhancement agents in MRI, targeted drug or gene delivery, tissue engineering, biological fluid detoxification, hyperthermia, biological sensing, nanozymes, cell labeling, and more [3-8]. Their biocompatibility and stability fill the niche of applications that require properties unattainable by organic materials. However, their use in some clinical applications is limited by low solubility and toxicity effects, as of May 2024, the clinicaltrials.gov system listed data on the development of 51 clinical protocols involving iron oxides NPs [9-11].

One of the major organs where the nanoparticles are likely to accumulate, depending on the route of administration, is the liver [12-14], where Kupffer cells can quickly uptake large nanoparticles (>100 nm), whereas smaller nanoparticles (<100 nm) are captured in the space of Disse, from where, if suitably functionalized, they can also accumulate in hepatocytes [15]. It has been shown that Fe_3O_4 NPs functionalized with

salicylic acid (35 mg/kg body weight) can accumulate in the liver and exhibit hepatotoxicity at a cumulative dose of more than 244 mg/kg over 28 days of exposure [16].

By controlling the physical properties of nanoparticles, it is possible to regulate their delivery and sequestration processes [17-20]. Depending on the size, coating, and duration of exposure, they can exhibit hepatotoxicity and cause inflammatory reactions [12, 21-24]. Askri et al. demonstrated the weakness of the antioxidant barrier against these iron nanoparticles [12]. After Fe_3O_4 NPs accumulate in lysosomes and release iron ions from their structure, it leads to the dysfunction of mitochondria, lysosomes, the Golgi apparatus, and the endoplasmic reticulum [25-26]. Wu and colleagues found that Fe_3O_4 NPs up to 5 nm in size can penetrate cells and initiate the Fenton reaction, resulting in the formation of the genotoxic •OH radical [6]. Moreover, iron overload in cells can lead to ferroptosis [27-28], whereas Fe_3O_4 NPs larger than 5 nm are unable to participate in these mechanisms [6].

Thus, the evaluation of the biocompatibility and hepatotoxicity of Fe_3O_4 NPs is currently relevant for their potential biomedical applications. The combination of phytotherapy with nanotechnology can enhance the pharmacological effectiveness by increasing the selectivity of action and reducing danger through lower dosages. Such approaches appear very promising, but it is essential to consider the risks of nanotoxicology, which studies the possible undesirable side effects of nanoparticles.

Combining phytopreparations with biocompatible nanoparticles allows for the delivery of biologically active phytocomponents to the target site with a lower likelihood of their biotransformation, significantly reducing the therapeutic dose of these agents [29-31]. The NPs themselves, possessing a certain spectrum of biological activities, contribute to the overall therapeutic and/or prophylactic effect. Therefore, the combined use of biocompatible NPs and medicinal plant extracts makes it potentially possible to

achieve breakthroughs in new approaches to the treatment and prevention of diseases. The development of such complexes is a relevant issue in biomedicine with significant potential for practical application.

In this work, we studied the biocompatibility and hepatotoxicity of Fe_3O_4 NPs both individually and in combination with the plant extract *T. polium* and its active component rutin on the liver of healthy white Wistar rats.

Results

The effects on liver function

Previous studies have identified pronounced biocompatible properties in the 70% ethanol extract of *Teucrium polium* (*T. polium)*, with an TFC value of 26.34 ± 0.11 µg/mL, IC_{50} equivalent to 1.40 ± 0.05 mg/mL, and HPLC detection of rutin (3.74 µg/mL) and genistein (0.21 µg/mL) [32]. In this study, we synthesized Fe_3O_4 NPs by a chemical method, characterized by a monocrystalline structure with a round shape and a diameter of 15 ± 4 nm [32-33]. Interaction of NPs with the extract and rutin leads to the formation of complexes, as demonstrated by spectral analysis [32].

The evaluation of hepatotoxicity based on ALT activity values revealed no direct hepatotoxicity from the agents tested in groups I (3.54 ± 0.7 U/L), II (7.07 ± 0.7 U/L), V (3.54 ± 0.7 U/L), and VI (3.54 ± 0.7 U/L) compared to the control. However, co-administration of the *T. polium* extract and Fe_3O_4 NPs (group III), as well as rutin and Fe_3O_4 NPs (group IV), resulted in increased ALT activity relative to normal values (up to 10.6 ± 0.7 U/L), by 2.1 and 3.3 times respectively (Fig. 1).

On the other hand, increases in AST activity relative to control values (5.3 ± 0.3 U/L) were observed in groups I (8.01 times), III (7.34 times), V (2 times), and even in group

VI (14.01 times), with values of 42.4 ± 0.3 U/L, 38.9 ± 0.3 U/L, 10.61 ± 0.3 U/L, and 74.26 ± 0.3 U/L, respectively (Fig. 2).

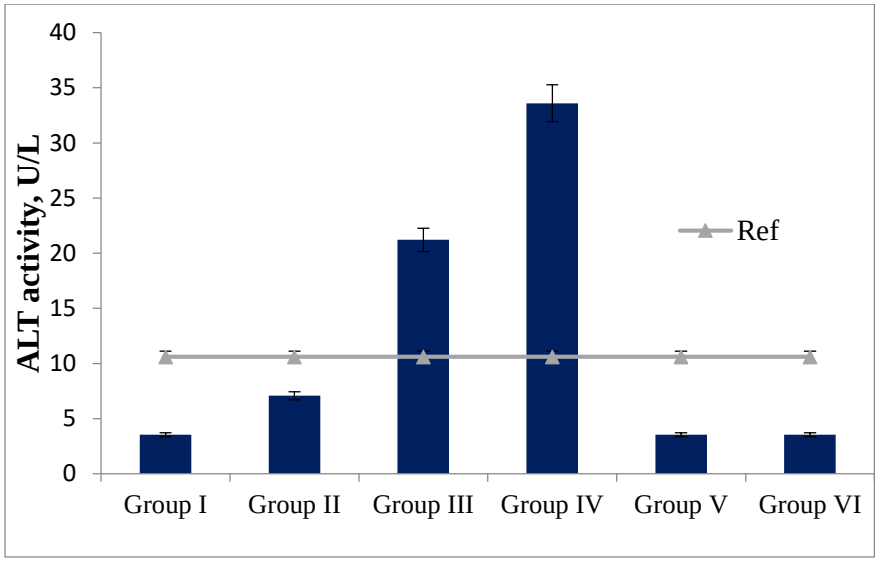

Figure 1. ALT activity (U/L) in the plasma of experimental animals ($p < 0.05$).

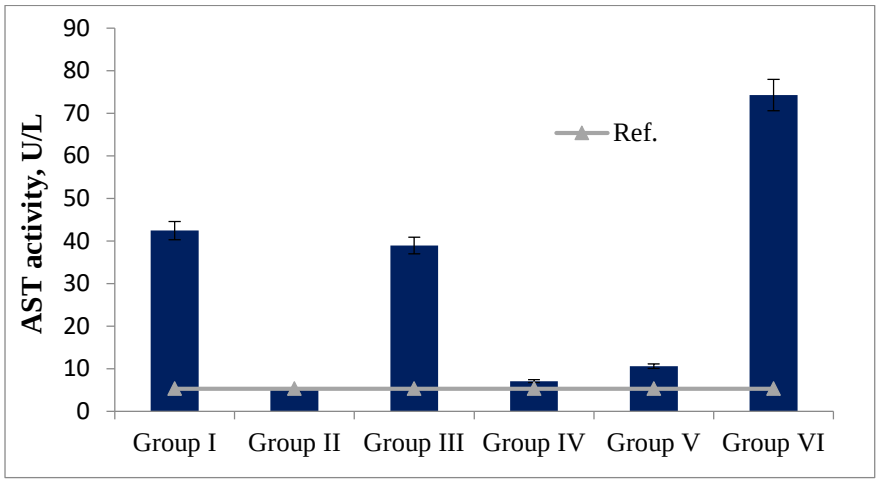

Figure 2. AST activity (U/L) in the plasma of all groups of experimental animals ($p < 0.05$).

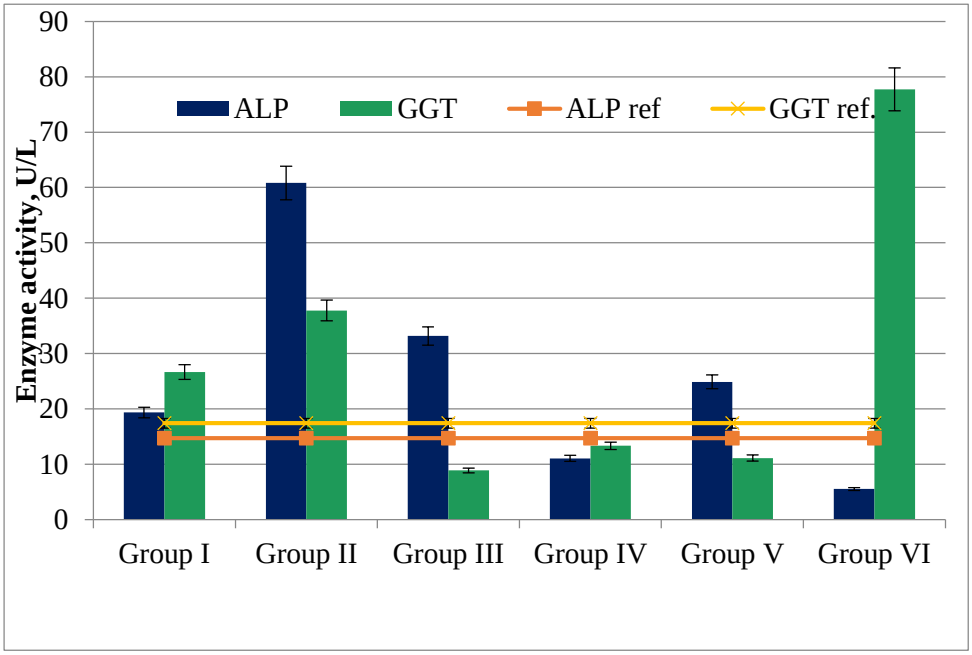

Figure 3. ALP and GGT activity (U/L) in the plasma of all groups of experimental animals ($p < 0.05$).

It can also be stated that in all groups, except for IV (11.06 ± 0.01 U/L) and VI (5.53 ± 0.03 U/L), there is an increase in ALP activity (Fig. 3) (normal range 14.7 ± 0.17 U/L). The greatest increase in enzyme activity is observed in group II (4.14 times), while a slightly lesser increase is observed in group III (2.26 times).

Against the backdrop of normal GGT activity values (17.42 ± 0.63 U/L), groups III (8.89 ± 0.43 U/L) and V (11.11 ± 0.07 U/L) show normal levels. However, in group IV, where the only agents involved were Fe_3O_4 NPs with rutin, there is no increase observed in either ALP (11.06 ± 0.01 U/L) or GGT (13.33 ± 0.14 U/L).

Assessment of the effect on lipid metabolism.

In the plasma of male Wistar rats in the control group, the normal level of total cholesterol reaches 2.87 ± 0.16 mM/L, HDL cholesterol is 0.8 ± 0.09 mM/L and higher, and LDL cholesterol is up to 2.07 ± 0.22 mM/L. According to these indicators, only in group I is the total cholesterol content close to normal values (Table 1). In the other groups, hypolipidemia is observed, with the maximum decrease in group IV. However, in some groups, there is an increase in HDL cholesterol (groups II, III, and VI), while in others, there is a decrease in HDL cholesterol (groups I, IV, and V), with almost identical minimal values in groups IV and V.

Table 1. Biochemical parameters of liver function in the plasma of experimental animals ($p < 0.05$).

	Control	Group I	Group II	Group III	Group IV	Group V	Group VI
Total cholesterol, mM/L	2,87± 0,16	2,1± 0,12	1,54± 0,06	1,26± 0,05	0,62± 0,04	1,01± 0,02	1,11± 0,03
HDL, mM/L	0,8± 0,09	0,58± 0,03	1,19± 0,04	1,16± 0,01	0,39± 0,03	0,34± 0,04	1,09± 0,03
LDL, mM/L	2,07± 0,22	1,52± 0,07	0,35± 0,01	0,100± 0,001	0,23± 0,02	0,67± 0,04	0,020± 0,001

Assessment of the impact on liver synthetic function.

In the control group of animals, the level of albumin is 29.33±1.3 g/L, and total protein is 45.23±1.43 g/L. In the control series of experiments, hyperalbuminemia is observed in groups III, IV, V, and VI according to this indicator (Table 2). Against this background, almost all groups, except for the II and V groups, also show an increase in total protein content. Increases against almost normal albumin levels are characteristic in pathological conditions when the total protein fraction increases due to acute phase proteins. Increases in total protein content may also be due to the release into the bloodstream of ALT, AST, ALP, and GGT enzymes.

Table 2. Biochemical parameters of liver function in the blood plasma of experimental animals in the control series ($p<0.05$).

	Control	**Group I**	**Group II**	**Group III**	**Group IV**	**Group V**	**Group VI**
Total protein, g/L	45,23± 1,43	55,59± 0,17	44,09± 0,09	52,51± 0,13	47,67± 0,08	42,11± 0,18	54,12± 0,31
Albumin, g/L	29,33± 1,3	28,39± 0,23	27,8± 0,35	34,14± 0,09	35,64± 0,14	31,74± 0,09	46,15± 0,26

Assessment of glutathione peroxidase (GPx) activity.

The highest GPx activity was detected in the liver homogenates of group V rats, where the enzyme activity was 15052±364 pkat/mg protein. This activity was 1.98 times higher compared to the GPx activity in healthy animal controls (up to 7624±281 pkat/mg protein) (Fig. 4). In all other groups, GPx activity was lower than in the control values. For instance, in group II, this value was 4581±172 pkat/mg protein, which was

1.66 times lower than that of the control. When the components of these groups were jointly applied, i.e., rutin with Fe3O4 NPs (group IV), GPx activity in the liver homogenates was almost absent. A similar pattern was observed in group I, where basal GPx activity was detected, not exceeding 896±93 pkat/mg protein, and in group VI, GPx activity in the homogenates was virtually absent.

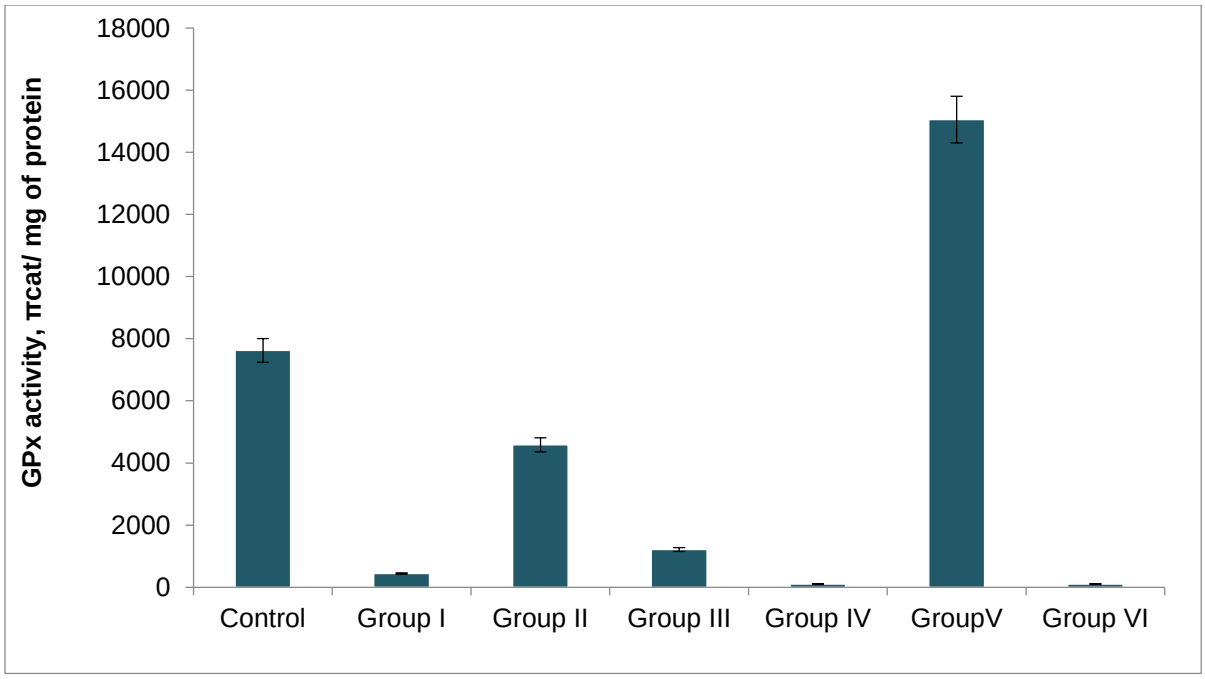

Figure 4. Activity of GPx in liver homogenates of experimental animals ($p < 0.05$).

Histological analysis of morphological changes in liver tissue.

In the histological examination of the toxic effects of the agents in all groups, a characteristic architecture typical of the liver was observed, with preserved lobular structure and radial arrangement of hepatocytes, as well as normal blood vessel filling (Fig. 5).

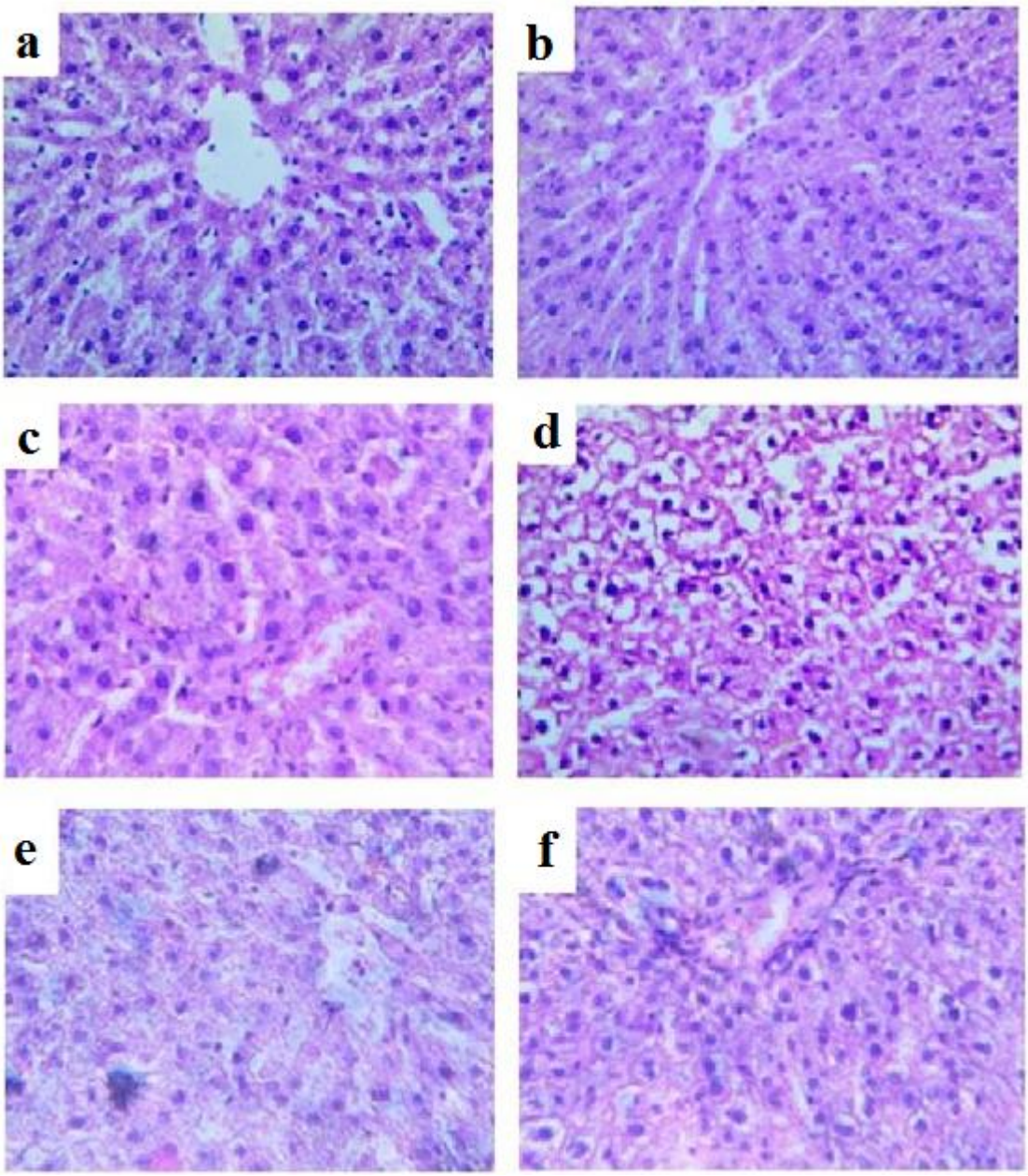

Figure 5. Microphotographs (ocular 20X, objective 100X) of liver tissue specimens from animals: a – *T. polium* extract, b – rutin, c –*T. polium* extract with Fe_3O_4 NPs, d – rutin with Fe_3O_4 NPs, e – Fe_3O_4 NPs, f - karsil.

However, in groups II and V, mildly pronounced dystrophic changes are observed in individual hepatocytes: cytoplasmic opacity and presence of optically distinguishable

vacuoles; whereas in group IV, these dystrophic changes are observed in the majority of hepatocytes.

DISCUSSION

Combining extracts with controlled biocompatible nanoparticles allows delivering biologically active components to the target site with a reduced likelihood of their biotransformation, thus significantly lowering the therapeutic dose of these agents [34-36]. Moreover, nanoparticles themselves contribute to the overall observed effect due to their specific spectrum of biological activities. Therefore, the development of such complexes and the identification of their biological properties spectrum are relevant issues in biomedicine with great potential for practical applications.

Previously, our studies have shown that spectral analysis of the composite of Fe_3O_4 NPs with 70% ethanol extract of *T. polium* revealed complex formation: leveling of peaks characteristic of the extract, as well as a hypochromic shift in the Fe_3O_4 NPs absorption spectrum [32].

The results of the impact of Fe_3O_4 NPs on liver tissue revealed practically no direct hepatotoxic properties. Increases in ALT and AST activities in some groups (Fig. 1, 2) may be associated with the effect of these agents, including on mitochondria of other cell types. Toxicity in cells leads to weakened mitochondrial activity, membrane leakage, and morphological changes. On the other hand, toxic NPs can adversely affect cell viability, proliferation rate, metabolic activity, and distort the therapeutic efficiency of the treatment [37]. The toxicity of NPs on biological entities fundamentally depends on the characteristics of the NPs, dose, and applications [4]. Thus, based on ALT/AST activity values, it can be concluded that Fe_3O_4 NPs do not exhibit pronounced toxic effects on the livers of healthy Wistar rats; however, when co-administered with

70% ethanol extract of *T. polium* and rutin, changes occur in the manifested complex activities.

It can also be stated that in all groups, except IV and VI, there is an increase in ALP activity (Fig. 3). This enzyme exists in the body in the form of 5 different isoforms with different localizations (liver, bile ducts, kidneys, bones, and placenta). Normally, plasma activity reflects only the hepatic isoform (14.7±0.17 U/L). However, against the backdrop of normal ALT values, an increase in ALP activity typically indicates a stagnation process in the bile ducts or a pathological process in the kidneys or bone tissue [38]. Comparing these data with the results of GGT activity determination (normal 17.42±0.63 U/L) allows determining the genesis of increased ALP activity (Fig. 3). Simultaneous elevation of both enzyme activities indicates localization of the pathological process in the bile ducts.

Against the backdrop of normal GGT activity in groups III and V, the increase in ALP activity may indirectly indicate the presence of a pathological process in other organs. Considering the fact that groups III and V received combined administration of Fe_3O_4 NPs, and the fact that many authors report the ability of these NPs to penetrate bone tissue, it can be assumed that the increase in plasma ALP activity is due to the bone isoform of this enzyme [38-39]. However, in group IV, where only Fe_3O_4 NPs with rutin were administered, no increase in either ALP or GGT was observed. Furthermore, according to literature data, the action of Fe_3O_4 NPs is dose-dependent, and Fe_3O_4 NPs (20-30 nm) administered to rat livers at doses up to 75 μg/g did not result in statistically significant changes in ALT, AST, and ALP activities [40].

One of the most important processes occurring in the liver, which characterizes its functional state, is lipid metabolism and lipoprotein synthesis. Based on the results showing a hypo-lipoproteinemic effect (Table 1), we hypothesize that one of the

possible intracellular molecular targets of such action of Fe_3O_4 NPs and its composites are proteins of the SIRT family, regulating the activity of PPARγ, PGC-1α, NF-kB, FOXO, p53, and others, as well as SREBP1c, whose increased activity in liver tissue leads to hypoactivation and suppression of cholesterol and triglyceride synthesis, as well as hyperexpression of GPx [45].

The increase in protein and albumin content in the plasma of experimental animals may be associated with the ability of xenobiotics to enhance the expression of transport proteins during prolonged exposure, correlating with studies by Belinskaia [46].

The combined effect of Fe_3O_4 NPs with 70% ethanol extract of *T. polium* and its component rutin leads to suppression of GPx activity, which may be associated either with the loss of this activity in the complex or with interaction with endogenous GPx and suppression of its antioxidant properties (Fig. 4). Fe_3O_4 NPs themselves are capable of increasing GPx activity, likely due to their peroxidase-like enzymatic properties (group V) [43]. This scenario correlates with literature data on the peroxidase-like enzymatic properties exhibited by Fe_3O_4 NPs, which is reflected in the preservation of liver tissue morphology but accompanied by changes in liver function biochemical markers (Figs. 1-3, Tables 1-2).

Considering the duration of exposure and the presence of noticeable dystrophic changes only in the group with maximum GPx suppression, it can be assumed that Fe_3O_4 NPs in combination with certain plant secondary metabolites may lead to excessive formation of free radicals, which underlie dystrophic changes.

Conclusion

The diversity of the obtained results is explained by the ability of Fe_3O_4 NPs to increase the bioavailability and intracellular concentration of associated components, thereby reducing their therapeutic dose and altering the profile of dose-dependent effects.

Additionally, both Fe_3O_4 NPs and their composites are presumed to interact with various spectra of intracellular structural regulators of biochemical processes.

Rutin and Fe_3O_4 NPs, individually, do not exhibit direct hepatotoxicity upon intraperitoneal administration in rats, unlike their complexes. Regarding lipid profiles, all agents tested induce a hypolipidemic effect through a reduction in LDL cholesterol, despite preserving liver synthetic functions. Fe_3O_4 NPs enhance GPx activity, which is attributed to their peroxidase-like enzymatic mimetic properties, while concurrently preserving the architecture of liver tissue.

Taking the above into account, it can be concluded that the effects of all investigated samples on liver tissue exhibit a multifaceted character and diverse mechanisms of activity. These mechanisms depend on the size of Fe_3O_4 NPs, hydrophilic shell diameter, solubility, aggregation, stability, and various other physicochemical and biological parameters. Given the importance and relevance of the issue, each of these factors requires close attention and further investigation. However, Fe_3O_4 NPs of spherical shape with a diameter ranging from 4 to 24 nm at a dose of 40 mg/kg may be recommended for further *in vivo* studies.

Experimental

Synthesis and characterization of iron oxide (Fe3O4) nanoparticales (supplementary)

The synthesis of iron oxide (Fe_3O_4) nanoparticles was carried out using a modified coprecipitation method with oleic acid as a stabilizer. 10 ml of 1M $FeSO_4*7H_2O$ and 10 ml of 2M $FeCl_3*6H_2O$ solutions were added to 10 ml 4M NaOH and 1 ml oleic acid. Then, the mixture was thoroughly mixed and heated at 80 °C for 1 h and color of the mixture turned from brown to black. The resulting black precipitate of Fe_3O_4 NPs was

washed three times with deionized water, then dispersed for 40 minutes in an ultrasonic disintegrator (Ultrasonic Homogenizer Sonic-150W, MRC, Israel) at 80% power with an on/off cycle of 5/4 seconds. During the synthesis of the nanoparticles, a black precipitate with paramagnetic properties formed. The nature and morphology of this precipitate were determined using electron diffraction and transmission electron microscopy (TEM) (LEO-912 abomega, Carl Zeiss, Germany) [32-33].

Preparation of plant extracts (supplementary)

T. polium were collected in August–September of 2016 in Kotayk marz (40°16′40″ N, 44°39′49″ E, height above sea level: 1445 m), Armenia (collection of the Department of Medical Biochemistry and Biotechnology). After a preliminary wash and sterilization in 1% calcium hypochlorite solution (Sigma Aldrich, Germany), plants were dried to 10% moisture level and grounded in a mechanical homogenizer to obtain a homogeneous powder.

For the preparation of extracts, the plant powder was mixed with the extragent, i.e. 96%, 70% and 50% ethanol, diluted in phosphate buffer (pH 7.4) in the 1:30 (w:v) ratio and exposed to ultrasound at 75 W (ultrasonic homogenizer, Sonic-150W, MRC, Israel). After 24-h incubation on the orbital shaker (60–70 rpm), the mixture was centrifuged for 15 min under 3000 rpm (Jouan GR412, France) [32].

HPLC analysis of plant extracts (supplementary)

To determine the major polyphenols, HPLC method was employed using a Waters Alliance 2695 chromatograph with a spectrophotometric and diode array detector, as well as MassLynx data processing software. Separation was done on a C-18 column (Knauer, Germany) (250 × 4 mm, particle size – 4.5 nm) at an elution rate of 1 ml/min with the following gradient elution system: HPLC grade water with 0.1% orthophosphoric acid (solution A) (Carlo Erba, France) – acetonitrile (solution B) (Carlo Erba, France); 0–5 min linear, solution A was adjusted from 10% to 40%, then to 50%

over the next 3 min and for the last 12 min, this ratio of solutions was maintained isocratic. Ethanol solutions of quercetin (Sigma Aldrich, Germany), rutin (Sigma Aldrich, Germany), apigenin (Sigma Aldrich, Germany), kaempferol (Sigma Aldrich, Germany) at 365 nm, naringenin (Sigma Aldrich, Germany) – 290 nm, genistein (Sigma Aldrich, Germany) – 261 nm and RA (Alfa Aeser, Germany) – 331 nm were used as standards [32].

Antiradical activity of extract (supplementary)

Antiradical activity (ARA) of the extract was measured by the colorimetric method using the stable radical 2,2-diphenyl-1-picrylhydrazyl (DPPH, Alfa Aeser, Germany) under the 30 °C. Optical density (OD) detection was carried out at 517 nm wavelength (UV-Vis 18, MRC, Israel), and ARA was estimated according to the following equation:

$ARA=(OD_c-OD_{sample}/OD_c-OD_{remnant})\times 100\%$,

where OD_c is the optical density of the control, OD_{sample} is the optical density of the sample and $OD_{remnant}$ is the remnant optical density of DPPH after its complete scavenging.

The IC_{50} value was determined from dose-dependent ARA curves as the concentration of components in the sample necessary for quenching 50% of the DPPH radicals [44].

Spectral analysis of sample complexes

The analysis of the spectra of the studied samples of 70% ethanol-buffer extract of *T. polium*, rutin, and their complexes with Fe_3O_4 NPs was carried out at wavelengths from 200 to 800 nm using a UV-Vis spectrophotometer UV-Vis 18 (MRC, Israel) [32].

Animal Experiment Modeling

Experiments were conducted on mature male white Wistar rats weighing 190-210 g. The animals were kept on a regular diet and water regimen at a temperature of 25±2ºC, 55±5% humidity, and a 12-hour day/night cycle. The animals were randomly divided

into 7 experimental groups of 5-6 individuals each, with intraperitoneal administration every 3 days for 2 months of 100 μL of the following agents:

Control - 70% ethanol-buffer solution

Group I - 70% ethanol-buffer extract of *T. polium* standardized by rutin content (1.87 μg/kg)

Group II - 70% ethanol-buffer solution of rutin (1.87 μg/kg)

Group III - Complex of Fe_3O_4 NPs (40 mg/kg) with 70% ethanol-buffer extract of *T. polium*

Group IV - Complex of Fe_3O_4 NPs (40 mg/kg) with rutin (1.87 μg/kg)

Group V - 70% ethanol-buffer suspension of Fe_3O_4 NPs (40 mg/kg)

Group VI - Drug "Karsil" (7 mg/kg)

A non-toxic dose of Fe_3O_4 NPs of 15±4 nm size was experimentally determined, considering the maximum permissible dose of 40 mg/kg in male laboratory mice [45]. All solutions of the agents were administered after being passed through antibacterial membrane filters (pore diameter 0.45 μm).

All interventions were performed in accordance with the principles of laboratory animal care of the Ethics Committee of Yerevan State Medical University (Yerevan, Armenia) and in accordance with the decision of 22 September 2010 of the Council of European Communities [2010/63/EU] and with the "ARRIVE" guidelines (Animals in Research: Reporting *In Vivo* Experiments). Euthanasia procedures were consistent with the recommendations of the American Veterinary Medical Association (AVMA) Guidelines on Euthanasia, using intraperitoneal injection of 70% ethanol [44].

For further biochemical analyses, blood was collected from the portal vein into vacutainers with the anticoagulant Na_2EDTA. For histological studies, part of each liver tissue sample was fixed in 10% formalin, and another part was placed in 10 mM K/P buffer (pH 7.2) at 4°C to study peroxidase enzyme activity.

Determination of Biochemical Markers of Liver Function

Biochemical analysis to determine the activities of alanine aminotransferase (ALT; EC 2.6.1.2), aspartate aminotransferase (AST; EC 2.6.1.1), gamma-glutamyl transferase (GGT; EC 2.3.2.2), and alkaline phosphatase (ALP; EC 3.1.3.1) in blood plasma, as well as the content of total protein (TP), albumin, total cholesterol (TC), HDL, and LDL, was carried out using standard BioSystems reagent kits (Barcelona, Spain) on a UV-Vis spectrophotometer UV-Vis 18 (MRC, Israel) according to the attached BioSystems protocols.

Determination of Glutathione Peroxidase Activity in Liver Tissue

To determine the activity of liver glutathione peroxidase (GPx) (EC 1.11.1.9), tissue samples weighing 1-2 g were homogenized in 10 mM potassium phosphate buffer (pH 7.2) on ice using a Potter-Elvehjem manual homogenizer. The tissue homogenate was then centrifuged for 15 minutes at 8000 g and 4°C. The resulting supernatant was used to determine liver GPx activity [46].

GPx activity was determined by detecting the accumulation of the pyrogallol oxidation product, purpurogallin, at 420 nm on a UV-Vis spectrophotometer UV-VIS 18 (MRC, Israel). Optical density was measured every 20 seconds for 3 minutes. The enzymatic mixture contained 0.8 ml of 10 mM K/P buffer (pH 7.2), 1.1 ml dH2O, 0.5 ml of 0.15% H_2O_2, and 0.5 ml of 2 mM pyrogallol. The enzymatic reaction was initiated by adding 0.12 ml of the liver tissue homogenate supernatant. GPx activity was defined as the formation of 1 mg of purpurogallin from pyrogallol in 20 seconds.

Liver GPx activity was calculated using the formula:

$A=\Delta D/t \cdot c$,

where A is the enzyme activity in pkat, ΔD is the change in optical density, tt is the measurement time in seconds, and c is the protein concentration. Protein concentration in the liver tissue homogenate supernatant was determined using the method described by [44].

Histological Analysis of Liver Tissue

Liver tissue samples, previously fixed in 10% formalin, dehydrated, and embedded in paraffin, were sectioned into 5 μm slices using a microtome. The liver tissue sections were stained with hematoxylin and eosin according to standard techniques【Ishii et al., 2016】. The histological preparations were analyzed using light microscopy on an AmScope microscope (USA), and microphotographs of the liver tissue samples were obtained using an AmScope MU500 5MP digital camera [44].

Statistical Analysis of Results

Statistical analysis was based on the comprehensive application of standard statistical methods, including the calculation of mean values, standard deviations, and standard errors of the mean. Biological replicates ranged from 4 to 6, with 2 to 3 series of experiments conducted for each. Tables, graphs, and diagrams present arithmetic means and their standard errors. Statistical analysis of the results was performed using one-way analysis of variance (ANOVA). Differences and correlations were considered significant at $p < 0.05$ (probability of error).

Acknowledgements

The authors thank Rshtuni L. (Russian-Armenian University) for assistance in conducting the experiments.

Funding

This research was funded by MESCS RA SC, grant number 10-2/24-I/RAU-BIOL, 21T-1F243.

References

1. Dye, C.; Acharya, S. How Can the Sustainable Development Goals Improve Global Health? A Call for Papers. *Bulletin of the World Health Organization* **2017**, *95* (10), 666–666A. https://doi.org/10.2471/blt.17.202358.

2. Zeshan Ali Sandhu; Muhammad Asam Raza; Abdulmajeed Alqurashi; Sajid, S.; Ashraf, S.; Imtiaz, K.; Aman, F.; Alessa, A. H.; Monis Bilal Shamsi; Latif, M. Advances in the Optimization of Fe Nanoparticles: Unlocking Antifungal Properties for Biomedical Applications. *Pharmaceutics* **2024**, *16* (5), 645–645. https://doi.org/10.3390/pharmaceutics16050645.

3. Vassallo, M.; Martella, D.; Barrera, G.; Federica Celegato; Coïsson, M.; Ferrero, R.; Olivetti, E. S.; Troia, A.; Hüseyin Sözeri; Parmeggiani, C.; Wiersma, D. S.; Tiberto, P.; Manzin, A. Improvement of Hyperthermia Properties of Iron Oxide Nanoparticles by Surface Coating. *ACS omega* **2023**, *8* (2), 2143–2154. https://doi.org/10.1021/acsomega.2c06244.

4. Huang, D.M.; Chung, T.H.; Hung, Y.; Lu, F.; Wu, S.H.; Mou, C.Y.; Yao, M.; Chen, Y.C. Internalization of Mesoporous Silica Nanoparticles Induces Transient but Not Sufficient Osteogenic Signals in Human Mesenchymal Stem Cells. *Toxicology and Applied Pharmacology* **2008**, *231* (2), 208–215. https://doi.org/10.1016/j.taap.2008.04.009.

5. Dong, H.; Du, W.; Dong, J.; Che, R.; Kong, F.; Cheng, W.; Ma, M.; Gu, N.; Zhang, Y. Depletable Peroxidase-like Activity of Fe3O4 Nanozymes Accompanied with Separate Migration of Electrons and Iron Ions. *Nature Communications* **2022**, *13* (1). https://doi.org/10.1038/s41467-022-33098-y.

6. Wu, L.; Wen, W.; Wang, X.; Huang, D.; Cao, J.; Qi, X.; Shen, S. Ultrasmall Iron Oxide Nanoparticles Cause Significant Toxicity by Specifically Inducing Acute Oxidative Stress to Multiple Organs. *Particle and Fibre Toxicology* **2022**, *19* (1). https://doi.org/10.1186/s12989-022-00465-y.

7. Somayeh Mikaeili Ghezeljeh; Salehzadeh, A.; Somayeh Ataei-e Jaliseh. Iron Oxide Nanoparticles Coated with Glucose and Conjugated with Safranal (Fe3O4@Glu-Safranal NPs) Inducing Apoptosis in Liver Cancer Cell Line (HepG2). *BMC chemistry* **2024**, *18* (1). https://doi.org/10.1186/s13065-024-01142-1.

8. Luong, T.; My Tran Diep; Ngoc Yen Nguyen; Duy Toan Pham; Hanh, N.; My, T. Alginate–Functionalized Fe3O4 Nanoparticles as a Drug Delivery System for Targeted Controlled Release. *Journal of drug delivery science and technology* **2024**, *93*, 105465–105465. https://doi.org/10.1016/j.jddst.2024.105465.

9. Mitchell, M. J.; Billingsley, M. M.; Haley, R. M.; Wechsler, M. E.; Peppas, N. A.; Langer, R. Engineering Precision Nanoparticles for Drug Delivery. *Nature Reviews Drug Discovery* **2020**, *20* (1), 1–24. https://doi.org/10.1038/s41573-020-0090-8.

10. Patra, J. K.; Das, G.; Fraceto, L. F.; Campos, E. V. R.; Rodriguez-Torres, M. del P.; Acosta-Torres, L. S.; Diaz-Torres, L. A.; Grillo, R.; Swamy, M. K.; Sharma, S.; Habtemariam, S.; Shin, H.-S. Nano Based Drug Delivery Systems: Recent Developments and Future Prospects. *Journal of Nanobiotechnology* **2018**, *16* (1). https://doi.org/10.1186/s12951-018-0392-8.

11. *Home - ClinicalTrials.gov*. www.clinicaltrials.gov. http://www.clinicaltrials.gov.

12. Askri; Cunin; Ouni; Béal; Rachidi; Sakly; Amara; Lehmann; Sève. Effects of Iron Oxide Nanoparticles (γ-Fe2O3) on Liver, Lung and Brain Proteomes Following Sub-Acute Intranasal Exposure: A New Toxicological Assessment in Rat Model Using ITRAQ-Based Quantitative Proteomics. *International Journal of Molecular Sciences* **2019**, *20* (20), 5186. https://doi.org/10.3390/ijms20205186.

13. Baboci, L.; Capolla, S.; Federica Di Cintio; Colombo, F.; Mauro, P.; Michele Dal Bo; Argenziano, M.; Cavalli, R.; Toffoli, G.; Paolo Macor. The Dual Role of the Liver in Nanomedicine as an Actor in the Elimination of Nanostructures or a Therapeutic Target. *Journal of oncology* **2020**, *2020*, 1–15. https://doi.org/10.1155/2020/4638192.

14. Colino, C. I.; Lanao, J. M.; Gutierrez-Millan, C. Targeting of Hepatic Macrophages by Therapeutic Nanoparticles. *Frontiers in Immunology* **2020**, *11*. https://doi.org/10.3389/fimmu.2020.00218.

15. Nowak-Jary, J.; Machnicka, B. *In Vivo* Biodistribution and Clearance of Magnetic Iron Oxide Nanoparticles for Medical Applications. *International Journal of Nanomedicine* **2023**, *Volume 18*, 4067–4100. https://doi.org/10.2147/ijn.s415063.

16. Bogdan Mîndrilă; Ion Rogoveanu; Sandra-Alice Buteică; Cercelaru, L.; Dan-Eduard Mihaiescu; Marina-Daniela Mănescu; Ion Mîndrilă; Ionica Pirici. Liver Histopathological Changes Related to Intraperitoneal Administration of Salicylic

Acid/Fe3O4 Nanoparticles to C57BL/6 Mice. *PubMed* **2022**, *48* (2), 146–154. https://doi.org/10.12865/chsj.48.02.02.

17. Joseph, T. M.; Kar Mahapatra, D.; Esmaeili, A.; Piszczyk, Ł.; Hasanin, M. S.; Kattali, M.; Haponiuk, J.; Thomas, S. Nanoparticles: Taking a Unique Position in Medicine. *Nanomaterials* **2023**, *13* (3), 574. https://doi.org/10.3390/nano13030574.

18. Yusuf, A.; Almotairy, A. R. Z.; Henidi, H.; Alshehri, O. Y.; Aldughaim, M. S. Nanoparticles as Drug Delivery Systems: A Review of the Implication of Nanoparticles' Physicochemical Properties on Responses in Biological Systems. *Polymers* **2023**, *15* (7), 1596. https://doi.org/10.3390/polym15071596.

19. Blanco, E.; Shen, H.; Ferrari, M. Principles of Nanoparticle Design for Overcoming Biological Barriers to Drug Delivery. *Nature biotechnology* **2015**, *33* (9), 941–951. https://doi.org/10.1038/nbt.3330.

20. Martínez-Ballesta, Mc.; Gil-Izquierdo, Á.; García-Viguera, C.; Domínguez-Perles, R. Nanoparticles and Controlled Delivery for Bioactive Compounds: Outlining Challenges for New "Smart-Foods" for Health. *Foods* **2018**, *7* (5), 72. https://doi.org/10.3390/foods7050072.

21. Ling, D.; Hyeon, T. Iron Oxide Nanoparticles: Chemical Design of Biocompatible Iron Oxide Nanoparticles for Medical Applications (Small 9-10/2013). *Small* **2013**, *9* (9-10), 1449–1449. https://doi.org/10.1002/smll.201370057.

22. Kusumoputro, S.; Au, C.; Lam, K. H.; Park, N.; Hyun, A.; Kusumoputro, E.; Wang, X.; Xia, T. Liver-Targeting Nanoplatforms for the Induction of Immune Tolerance. *Nanomaterials* **2023**, *14* (1), 67–67. https://doi.org/10.3390/nano14010067.

23. Sanjib Kumar Das; Sen, K.; Ghosh, B.; Ghosh, N.; Sinha, K.; Sil, P. C. Molecular Mechanism of Nanomaterials Induced Liver Injury: A Review. *World journal of hepatology* **2024**, *16* (4), 566–600. https://doi.org/10.4254/wjh.v16.i4.566.

24. Abbasi, R.; Shineh, G.; Mobaraki, M.; Doughty, S.; Tayebi, L. Structural Parameters of Nanoparticles Affecting Their Toxicity for Biomedical Applications: A Review. *Journal of Nanoparticle Research* **2023**, *25* (3). https://doi.org/10.1007/s11051-023-05690-w.

25. Chaves, N.; Estrela-Lopis, I.; Böttner, J.; Lopes, C. A. P.; Cândido Guido, B.; Souza, A.; Bao, S. Exploring Cellular Uptake of Iron Oxide Nanoparticles Associated with Rhodium Citrate in Breast Cancer Cells. *International Journal of Nanomedicine* **2017**, *Volume 12*, 5511–5523. https://doi.org/10.2147/ijn.s141582.

26. Liu, P. F.; Liu, D.; Cai, C.; Chen, X.; Zhou, Y.; Wu, L.; Sun, Y.; Dai, H.; Kong, X.; Xie, Y. Size-Dependent Cytotoxicity of Fe_3O_4 Nanoparticles Induced by Biphasic Regulation of Oxidative Stress in Different Human Hepatoma Cells. *International Journal of Nanomedicine* **2016**, *Volume 11*, 3557–3570. https://doi.org/10.2147/ijn.s105575.

27. Huang, Q.-T.; Hu, Q.-Q.; Wen, Z.-F.; Li, Y.-L. Iron Oxide Nanoparticles Inhibit Tumor Growth by Ferroptosis in Diffuse Large B-Cell Lymphoma. *American Journal of Cancer Research* **2023**, *13* (2), 498–508.

28. Fernández-Acosta, R.; Iriarte-Mesa, C.; Alvarez-Alminaque, D.; Behrouz Hassannia; Wiernicki, B.; Díaz-García, A. M.; Vandenabeele, P.; Tom Vanden Berghe; Lázaro, G. Novel Iron Oxide Nanoparticles Induce Ferroptosis in a Panel of Cancer Cell Lines. **2022**, *27* (13), 3970–3970. https://doi.org/10.3390/molecules27133970.

29. LI, C.; ZHANG, J.; ZU, Y.-J.; NIE, S.-F.; CAO, J.; WANG, Q.; NIE, S.-P.; DENG, Z.-Y.; XIE, M.-Y.; WANG, S. Biocompatible and Biodegradable Nanoparticles for Enhancement of Anti-Cancer Activities of Phytochemicals. *Chinese Journal of Natural Medicines* **2015**, *13* (9), 641–652. https://doi.org/10.1016/s1875-5364(15)30061-3.

30. Chavda, V. P.; Nalla, L. V.; Balar, P.; Bezbaruah, R.; Apostolopoulos, V.; Singla, R. K.; Khadela, A.; Vora, L.; Uversky, V. N. Advanced Phytochemical-Based Nanocarrier Systems for the Treatment of Breast Cancer. *Cancers* **2023**, *15* (4), 1023. https://doi.org/10.3390/cancers15041023.

31. Yusuf, A.; Almotairy, A. R. Z.; Henidi, H.; Alshehri, O. Y.; Aldughaim, M. S. Nanoparticles as Drug Delivery Systems: A Review of the Implication of Nanoparticles' Physicochemical Properties on Responses in Biological Systems. *Polymers* **2023**, *15* (7), 1596. https://doi.org/10.3390/polym15071596.

32. Kazaryan, Sh. A.; Rshtuni, L. R.; Hovhannisyan, A. A. The Synergistic Antibacterial Activity of Silver Nanoparticles and T. Polium Extracts. *Biophysics* **2021**, *66* (4), 623–628. https://doi.org/10.1134/s0006350921040084.

33. Gabrielyan, L.; Hovhannisyan, A.; Gevorgyan, V.; Ananyan, M.; Trchounian, A. Antibacterial Effects of Iron Oxide (Fe3O4) Nanoparticles: Distinguishing Concentration-Dependent Effects with Different Bacterial Cells Growth and Membrane-Associated Mechanisms. *Applied Microbiology and Biotechnology* **2019**, *103* (6), 2773–2782. https://doi.org/10.1007/s00253-019-09653-x.

34. Sérgio Antunes Filho; Santana; Santos; Bianca Pizzorno Backx; Soran, M.-L.; Ocsana Opriş; Lung, I.; Stegarescu, A.; M. Bououdina. Biosynthesis of Nanoparticles Using Plant Extracts and Essential Oils. *Molecules* **2023**, *28* (7), 3060–3060. https://doi.org/10.3390/molecules28073060.

35. Adeyemi, J. O.; Oriola, A. O.; Onwudiwe, D. C.; Oyedeji, A. O. Plant Extracts Mediated Metal-Based Nanoparticles: Synthesis and Biological Applications. *Biomolecules* **2022**, *12* (5), 627. https://doi.org/10.3390/biom12050627.

36. Liao, C.; Li, Y.; Tjong, S. Bactericidal and Cytotoxic Properties of Silver Nanoparticles. *International Journal of Molecular Sciences* **2019**, *20* (2), 449. https://doi.org/10.3390/ijms20020449.

37. Yang, C.-Y.; Hsiao, J.-K.; Tai, M.-F.; Chen, S.-T.; Cheng, H.-Y.; Wang, J.-L.; Liu, H.-M. Direct Labeling of HMSC with SPIO: The Long-Term Influence on Toxicity, Chondrogenic Differentiation Capacity, and Intracellular Distribution. *Molecular Imaging and Biology* **2010**, *13* (3), 443–451. https://doi.org/10.1007/s11307-010-0360-7.

38. Lu, D.; Wu, X.; Wang, W.; Ma, C.; Pei, B.; Wu, S. Synthesis and Application of Iron Oxide Nanoparticles in Bone Tissue Repair. *Journal of Nanomaterials* **2021**, *2021*, e3762490. https://doi.org/10.1155/2021/3762490.

39. Chung, E.; Rylander, M. N. Response of a Preosteoblastic Cell Line to Cyclic Tensile Stress Conditioning and Growth Factors for Bone Tissue Engineering. *Tissue Engineering Part A* **2012**, *18* (3-4), 397–410. https://doi.org/10.1089/ten.tea.2010.0414.

40. Parivar, K.; Malekvand Fard, F.; Bayat, M.; Alavian, S. M.; Motavaf, M. Evaluation of Iron Oxide Nanoparticles Toxicity on Liver Cells of BALB/c Rats. *Iranian Red Crescent Medical Journal* **2016**, *18* (1). https://doi.org/10.5812/ircmj.28939.

41. Moslehi, A.; Hamidi-zad, Z. Role of SREBPs in Liver Diseases: A Mini-Review. *Journal of Clinical and Translational Hepatology* **2018**, *6* (3), 332–338. https://doi.org/10.14218/JCTH.2017.00061.

42. Belinskaia, D. A.; Voronina, P. A.; Goncharov, N. V. Integrative Role of Albumin: Evolutionary, Biochemical and Pathophysiological Aspects. *Journal of Evolutionary Biochemistry and Physiology* **2021**, *57* (6), 1419–1448. https://doi.org/10.1134/s002209302106020x.

43. Dong, H.; Du, W.; Dong, J.; Che, R.; Kong, F.; Cheng, W.; Ma, M.; Gu, N.; Zhang, Y. Depletable Peroxidase-like Activity of Fe3O4 Nanozymes Accompanied with Separate Migration of Electrons and Iron Ions. *Nature Communications* **2022**, *13* (1). https://doi.org/10.1038/s41467-022-33098-y.

44. Kazaryan, S.; Farsiyan, L.; Tumoyan, J.; Kirakosyan, G.; Ayvazyan, N. M.; Gasparyan, H. V.; S. Buloyan; Lilit Arshakyan; Kirakosyan, A.; Hovhannisyan, A. Oxidative Stress and Histopathological Changes in Several Organs of Mice Injected with Biogenic Silver Nanoparticles. **2022**, *50* (1), 331–342. https://doi.org/10.1080/21691401.2022.2149931.

45. Farsiyan, L. M.; Kazaryan, S. A.; Hovhannisyan, A. A. Comparative Analysis of Iron Oxide Nanoparticle's (Fe3O4) Cytotoxicity Synthesized by Chemical and Biogenic Methods. *IFMBE proceedings* **2022**, 48–54. https://doi.org/10.1007/978-3-030-92328-0_7.

46. Arutyunyan, A. A.; Hovhannisyan, A. A.; Kazaryan, S. H. A.; Tiratsuyan, S. G. Effect of Silver Nanoparticles on Peroxidase Activity of Linum Ausriacum L. And Hypericum Perforatum L. Callus Culture. *Toxicon* **2019**, *159*, S21. https://doi.org/10.1016/j.toxicon.2018.11.387.